

Heat Transfer and Pressure Drop Performance Comparison of Finned-Tube Bundles in Forced Convection

RENE HOFMANN , FRIEDRICH FRASZ, KARL PONWEISER

Institute of Thermodynamics and Energy Conversion

Vienna University of Technology

A-1060 Vienna, Getreidemarkt 9/E302

AUSTRIA

Rene.Hofmann@tuwien.ac.at <http://www.ite.tuwien.ac.at>

Abstract: In this paper, heat transfer and pressure drop at different transverse serrated and solid finned-tubes were investigated in cross-flow with aim of optimizing heat exchanger performance. Three different finned-tube shapes were investigated. The I-shaped and U-shaped fin geometries under consideration have varying geometrical constants, i.e. fin height, fin pitch, fin thickness, and fin width. The heat exchanger consists of eight consecutive finned-tube rows and eleven tubes on top of each other. The finned tubes are arranged in a staggered formation at equal transverse and longitudinal pitch. The experimental setup, measurement technique and measurement uncertainties are presented. The design of an optimum heat exchanger must take into account the advantages and disadvantages of geometrical factors which influence heat transfer and pressure drop. After measurement validation, the derived correlations for the Nusselt number and the pressure drop coefficient were compared with experimental results and equations from literature. The difference between solid and serrated finned tubes is shown with the help of equations for a special configuration from literature. Additionally, a performance evaluation criterion for single-phase flows, developed by Webb [14], was carried out for the three different serrated and solid fin geometries. To evaluate the uncertainty of pressure drop measurement, the analogy to the “generalized L ev eque equation” cited in Martin and Gnielinski [13] was used.

Key-Words: Finned tube, Heat transfer, Pressure drop, Serrated fin, Solid fin, Performance evaluation criterion, Experimental setup, L ev eque Analogy, Turbulent flow, Helical finned tubes

1 Introduction

The reduction of primary energy sources is claimed to improve the efficiency of heat exchangers. This is also a contribution to the reduction of CO₂ production. Whenever gas/water heat exchangers are used, the heat transfer coefficient α_0 on the air side of air/water tube heat exchangers, e.g. steam boilers or heat recovery boilers, is inherently lower than the heat transfer coefficient on the inside of the water tubes. Finned tubes are applied to enhance heat transfer. There are many possibilities for improving heat transfer on the air side. On the one hand, the heat-transferring surface can be enlarged by an arrangement of annular fins or other elements. This increase of total tube surface allows transfer of a greater amount of heat from hot gas, but the demand for smaller installation sizes requires smaller fin pitch with larger fin height. On the other hand, finned tubes with segmented fins show somewhat higher turbulence than those with smooth fins since the boundary layer has to be established at each individual segment [8]. Staggered arrangement of the tubes in the bundle also increases turbulence. A higher pressure drop is caused by resistance in the flow channel and turbulence. Optimizing a finned-

tube heat exchanger also results in minimizing the pumping power. Experimental investigations at solid and serrated finned-tubes have been studied extensively by [2], [6], [7], [9], [10], [11], [27], [28], [29], and [31]. Taborek [1] and Frasz [6] compared the varying influences of solid and segmented fins, while Weierman [3] investigated the performance of in-line and staggered tube arrangement of segmented finned tubes. Weierman and Taborek found that in-line arrangement should only be used for special cases because of the disadvantage of possible bypass flow between the tube bundles. On the other hand, staggered arrangement of tubes in the flow channel can cause a higher pressure drop. Bell and Kegler [30] analyzed mathematically the effect of bypassing in heat exchangers for a specific thermal performance. Genic [18] investigated experimentally the pressure drop of in-line and staggered arrangements and compared these correlations with the literature. Rabas and Eckles [19] investigated seven different segmented finned-tube bundle arrangements. They ascertained that, compared to solid fins, the fin height of segmented fins can be greater than the maximum fin height because such fins are easier to laser-weld. This

would increase the total outside surface area and as a result the efficiency of the heat exchanger. Briggs and Young investigated several finned-tube configurations. The given heat transfer correlation is based on tubes varying widely with respect to fin height, fin thickness, fin spacing and root diameters [28]. These equations can be used for predicting six-row deep tube banks with solid fins. Ward and Young developed heat transfer and pressure drop correlations for plain finned tubes with triangular pitch. They compared their pressure drop data with a correlation from literature [29]. Breber [31] presents a review and evaluation of heat transfer and pressure drop predictive method for tube bundles with stud fins.

Geometrical effects e.g. row effects on heat transfer and pressure drop have been observed in literature. In addition, correction factors have been introduced and a relationship between heat transfer and pressure drop, depending on the tube row number, established. The influence on heat transfer of the number of tube rows, arranged consecutively, was investigated in [27]. Necula, Nineta, and Darie [25] experimentally studied the influence of rows in cross-flow heat exchangers. They compared their results with theoretical correlations. All measurements were performed in the Reynolds range between 10000 and 30000.

Numerous correlations for the prediction of heat transfer of serrated fin tubes have been derived by [5], [7] and [15], whereas Nir's [5] correlations are based on a large amount of heat-transfer and pressure-drop data. Kawaguchi [7] specifies an accuracy level of $\pm 5\%$ for the equations used to predict the Nusselt number and the friction factor. Weierman's [2] correlations for heat transfer in a staggered layout show an expected accuracy of $\pm 10\%$; and for the pressure-drop equations an accuracy level of $\pm 15\%$ is achieved.

Heat transfer and pressure drop equations are functions of the geometrical parameters i.e. fin height, fin pitch, fin thickness, fin width, fluid properties, variables of state etc. In order to calculate the overall heat transfer of a finned tube, according to the laws of heat conduction and heat convection the fin efficiency, as a reduction coefficient, has to be considered. Hashizume et al. [12] calculated the fin efficiency of serrated fins using an analytical model, with the assumption of a heat transfer coefficient uniformly distributed over the fin surface and the segmented section, as well as a second equation for theoretical fin efficiency. Spine-fin efficiency with a variable cross-sectional area was calculated in [24] and [26] analytically using Bessel functions in a closed form equation.

Fin efficiency has been developed for a steady-state energy balance and specified fin-tip conditions. Kearney and Jacobi [4] investigated experimentally local heat transfer behaviour in staggered and in-line arrangements with the help of optical adaptation of the naphthalene sublimation technique in order to evaluate the analytical fin efficiency.

In Webb [20], an excellent overview of plate fin and circular finned tube studies is presented. Factors such as fin spacing, fin efficiency and fin configuration yield enhanced heat transfer. Yet one finned-tube heat exchanger study claims to maximize the heat transfer rate while simultaneously minimizing pumping power. Webb [14] as well as Stephan and Mitrović [16] developed criteria for the evaluation of the performance of a heat exchanger in order to quantify the heat output capacity while considering the pumping power.

In the present paper the performance of various finned tubes in forced convection was evaluated. Three types of finned tubes were investigated where the fin height varies most. The influence of geometry on heat transfer and pressure drop properties was compared for solid and serrated I-shaped fins and serrated U-shaped fins. In particular, the influence of fin height was considered. In addition, the analogy to the "generalized L  v  que equation" for heat transfer correlations was applied.

2 Experimental Setup

2.1 Test facility

A test rig for heat transfer and pressure-drop measurements on finned-tube bundles in cross-flow is in operation at the laboratory of the Institute for Thermodynamics and Energy Conversion at the Vienna University of Technology. This test facility allows measurement at Reynolds numbers in the range between 4500 and 35000 and flue gas mass-flow from 0.6 to 4.5 kg/s; the layout is shown in Figure 1. The finned-tube bundle is admitted with hot gas of up to 400  C which is generated by combustion of natural gas. Air intake is performed using a Venturi nozzle and a smaller ISA 1932 inlet nozzle for low Re numbers, which are also used for mass flow measurement of combustion air. Both systems were pre-calibrated before application.

Following a connecting section with a bend, a variable incidence entry vane is mounted in front of the radial fan for mass flow regulation of the air. The radial fan can produce a maximum pressure of 5000 Pa and generates 45000 Nm³/h at 3500 Pa. The air flows through a three-meter conical connecting

piece to the burner. The burner is designed as a duct burner, drawing its combustion air partly from the process air through ductings. Maximum burner power is 1160 kW. Downstream from the burner is a tube with a diameter of 600 mm, in which a static mixer application is installed.

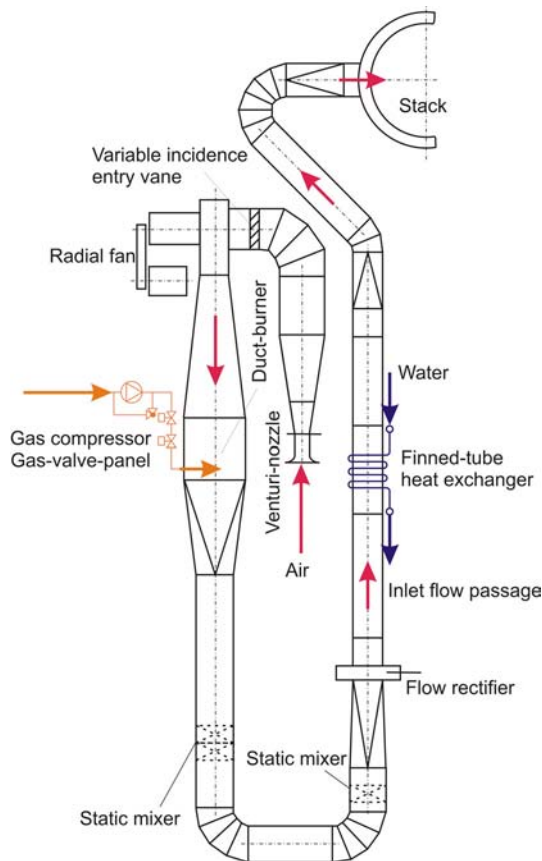


Fig.1: Layout and design of the test facility

After two 90° bends there is an additional mixer application, followed by a transition piece to a rectangular cross-section, 500 mm in width and 1000 mm in height, containing a flow rectifier consisting of three fine-wire meshes in close arrangement. After the flow rectifier, which rectifies the vortices caused by mixers and redirecting pipes, a 2000 mm inlet channel follows, which serves to calm the fully developed turbulent flow. The finned-tube heat exchanger with a tube length of approx. 500 mm is built into a 1500 mm channel section. Downstream from this testing channel, the flue gas is conducted into a steel tube stack. The finned-tube heat exchanger consists of a rectangular sheet-steel channel in which the finned tubes are arranged horizontally with a given transversal and longitudinal pitch. The free channel width is fixed at 500 mm.

All connecting pipes are arranged at the outside of the channel. This is the only arrangement allowing exact measurement of heat transfer at the small test section width of the tube banks. Measurements are thus not influenced by bypass flow through the space for the bends.

The volume flow of water is constant with $V_w=14.1 \text{ m}^3/\text{h}$ at $p_w=2.7 \text{ bar}$ and a velocity of $w_w=0.5 \text{ m/s}$. The tube bundle consists of 88 tubes which are arranged in 8 consecutive columns consisting of 11 horizontal tubes each. An even cooling water flow distribution in the tubes is achieved by orifices after the inlet collector. The hot parts of the test facility are insulated using mineral wool, glass wool and aluminum foil to prevent heat loss. For more details see [8].

2.2 Measurement procedure

The experimental investigation requires a number of measurements to be taken simultaneously in order to evaluate and determine the amount of transferred heat as well as gas-side pressure drop. A diagram of the measurement application is presented in Figure 2. The temperatures on the water side are measured for every coiled tube at the inlet and at the outlet using Pt-100 RTDs (resistance temperature detectors) so that fringe effects can be ascertained for the outside tubes and considered in the evaluation.

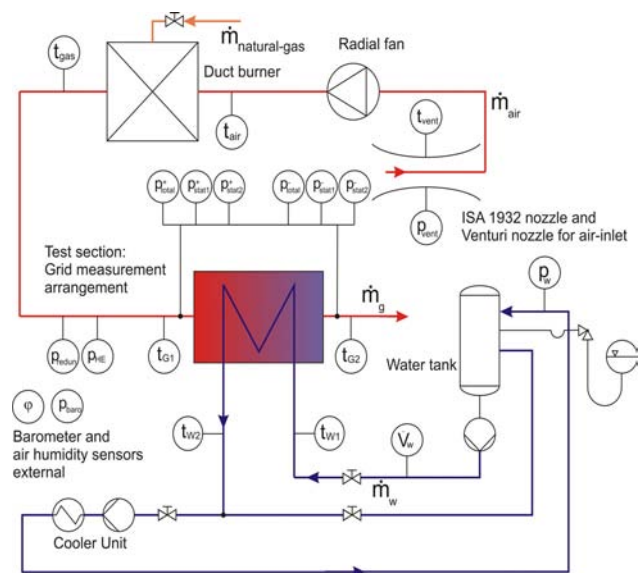


Fig.2: Measurement application

Gas temperatures are measured using NiCr-Ni thermocouples. In order not to significantly affect the flow pattern, the diameter of these thermocouples was chosen to be only 1.5 mm. Four thermocouples are arranged and mounted in front of

and behind the heating surface of the heat exchanger to obtain a grid measurement. Three NiCr-Ni thermocouples measure the air temperature at the Venturi nozzle and after the fan as well as the gas temperature after the burner. The mass flow of water is measured using a calibrated hot water meter with an electronic sensor.

The mass flow of air is measured by determining the pressure difference at the Venturi nozzle in front of the inlet collector using two different sensors: a Honeywell micro-switch series 160 ($\pm 0.25\%$ Full scale (FS)) and a Furness Controls micro-manometer. The air humidity is measured by means of an electronic humidity sensor. The barometric pressure is measured using a Honeywell HPB digital precision barometer with an accuracy of ± 0.4 hPa FS. The static pressure differences at the air side of the finned-tube bundle are measured at four inlets in front of and behind the heating surface of the heat exchanger to obtain a grid measurement using a Honeywell PPT digital precision pressure transducer with an accuracy of $\pm 0.05\%$ FS.

The total pressure difference at the centre of the combustion channel is measured using a United Sensor pitot-static pressure probe. The absolute pressure in the combustion channel is measured using a Honeywell micro-switch series 160 ($\pm 0.25\%$ FS). All measurement systems were pre-calibrated before application. The measured values are transmitted to the process computer using measurement value periphery by National Instruments and the LabView 7E program system.

2.3 Measurement uncertainties

The heat transfer coefficient at the inner side of the tube is calculated by knowing all data on the water side. The mass flow of water is constant but with a given uncertainty. Using the logarithmic mean temperature difference and the fluid properties, the heat transfer coefficient on the gas side can be calculated. Upon applying the law of error propagation by Gauss to the mass flow measurement of air, the measurement uncertainties calculate as follows: the results show a disproportionate increase at low Re numbers ($Re < 14000$). The average error of the mass flow measurement of air is about $\pm 3\text{-}5\%$. At $Re = 10000$ the uncertainty is about $\pm 10\%$, and for $Re < 7000$ about $\pm 15\%$ (see Figure 3). Thus, at low Re numbers an ISA 1932 inlet nozzle was applied with almost linear measurement uncertainty distribution resulting. In addition, at low Re numbers while using the Venturi nozzle a micro-manometer (meter scale ± 19.99 mm H₂O) was applied to reduce measurement uncertainties.

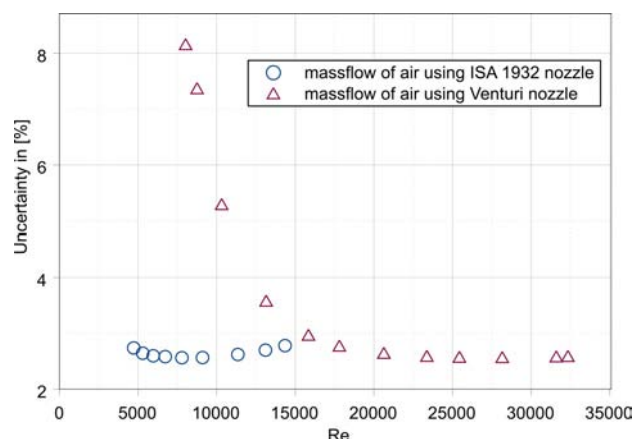


Fig.3: Uncertainties of mass flow measurement

3 Analyzed finned tubes

Three different finned-tube geometries have been tested and analyzed in order to characterize the influence on heat transfer and pressure drop and thus to optimize heat-exchanger geometry. The tubes tested, with solid and serrated I-shaped and serrated U-shaped fin geometry, are specified in Table 1.

Fin Geometry	I-shaped, solid	I-shaped, serrated	U-shaped, serrated
Bare tube diameter	38.0 mm	38.0 mm	38.0 mm
Tube thickness	2.6 mm	4 mm	3.2 mm
Number of fins per m	276	276	295
Average fin height	15 mm	15.5 mm	20.0 mm
Average fin thickness	1.0 mm	1.0 mm	0.8 mm
Average tube length	500 mm	500 mm	495 mm
Average segment width	-	4.5 mm	4.3 mm
Number of tubes in the direction of flow	8	8	8
Number of tubes per row	11	11	11
Longitudinal tube pitch	79 mm	79 mm	79 mm
Transversal tube pitch	85 mm	85 mm	85 mm
Total outside surface area of the bundle	67.06 m ²	64.05 m ²	84.48 m ²
Fin material	St 4	St 37.2	DC01
Tube material	St 35.8	St 35.8	St 35.8
Net free area of tube row	0.234 m ²	0.2326 m ²	0.2292 m ²

Table 1: Specifications of finned tubes

All investigated tube banks have the same transversal and the same longitudinal pitch. The net free area in a tube row is almost equal for the various investigated geometries. The geometrical fin height constant varies the most (I-shaped fin 15 mm and U-shaped fin 20 mm). Thus the total outside surface area of the U-shaped finned tube is larger than that of the I-shaped fin tubes.

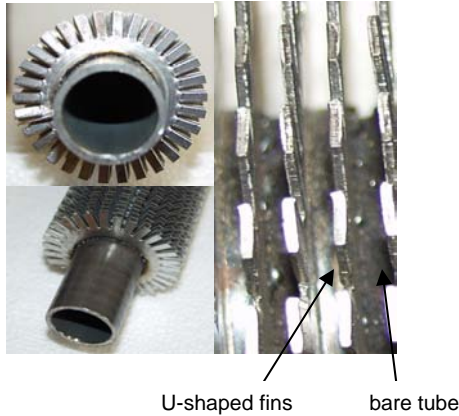


Fig.4: Experimental tube with U-fins

The main advantages of the segmented U-shaped fin geometry (Figure 4) are larger contact area between fin and tube (heat conduction) and the possibility of closer fin spacing, which allows a larger total outside surface area at equal fin height of the bundle. Thus, an equally small or smaller installation size of the heat exchanger can be achieved. Figure 5 shows the different fin types and the differences in contact area.

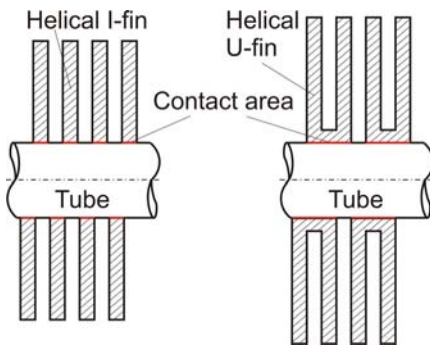


Fig 5: Contact area of I-shaped and U-shaped finned tubes

4 Data reduction and interpretation

4.1 Governing heat transfer equations

The heat transfer rate of water is determined directly by

$$\dot{Q} = \dot{m}_w (h_{w_2} - h_{w_1}) . \tag{1}$$

The heat transfer rate of the combustion gas is defined by

$$\dot{Q} = \dot{m}_g c_{p_g} (T_{g_1} - T_{g_2}) . \tag{2}$$

Heat conduction through the tube wall is known as

$$\dot{Q} = k A_{tot} \Delta T_{ln} , \tag{3}$$

where k is the heat transfer coefficient of conduction, A_{tot} the total outside surface area of the bundle and ΔT_{ln} the logarithmic mean temperature difference between input and output of the heat exchanger:

$$\Delta T_{ln} = \frac{(T_{g_1} - T_{w_2}) - (T_{g_2} - T_{w_1})}{\ln \frac{T_{g_1} - T_{w_2}}{T_{g_2} - T_{w_1}}} . \tag{4}$$

In the current study, the LMTD is calculated using the equation for counter-flow heat exchangers. For a large number of consecutive tube rows, the difference between counter-flow and counter cross-flow in the formula for calculating the logarithmic mean temperature difference is small and may thus be neglected.

For calculating the heat transfer of a finned tube, convection and heat conduction have to be considered. A reduction coefficient termed “fin efficiency” is therefore introduced, by which the actual heat transfer coefficient is multiplied in order to obtain the apparent heat transfer coefficient. Fin efficiency is calculated according to the laws of heat conduction under the assumption that the actual heat transfer coefficient is uniformly distributed across the fin surface [8]. The apparent heat transfer coefficient is

$$\alpha = \frac{1}{\frac{1}{k} - f_a \frac{d_a}{d_i \alpha_i} - f_a \frac{d_a}{2\lambda_r} \ln \frac{d_a}{d_i}} . \tag{5}$$

Fin efficiency is calculated according to [23]. η_{r1} is the fin efficiency for the radian part including the segment. η_{r2} is the fin efficiency for the radian part without the segment (see Figure 3); from knowing the reduced fin height h_{red} it follows that

$$\eta_{r1} = \frac{\tanh(m_1 h_{red})}{m_1 h_{red}} \quad (6)$$

$$\eta_{r2} = \frac{\tanh(m_2 h_{red2})}{m_2 h_{red2}}. \quad (7)$$

The parameters m_1 and m_2 are defined as follows:

$$m_1 = \sqrt{\frac{2\alpha_0 b_s + s}{\lambda_{ri} s b_s}} \quad (8)$$

$$m_2 = \sqrt{\frac{2\alpha_0}{\lambda_{ri} s}}. \quad (9)$$

where λ_{ri} is the thermal conductivity of the fin and b_s the segment width. The reduced fin height is calculated according to the method of T. E. Schmidt [23], [6], and [8] separately for the radian part with and without the segment. In this case h_{red} and h_{red2} are defined as follows:

$$h_{red} = h_B \left(1 + 0.35 \ln \left(\frac{d_a + 2h}{d_a} \right) \right) + \left[h_s + \frac{s}{2} \right] \quad (10)$$

$$h_{red2} = \left(h_B + \frac{s}{2} \right) \left(1 + 0.35 \ln \left(\frac{d_a + 2h}{d_a} \right) \right). \quad (11)$$

If equations (8) and (9) are applied to (6) and (7) with (10) and (11), overall fin efficiency η_r calculates as follows

$$\eta_r = \eta_{r1} \frac{d_a + h}{d_a + 2h} + \eta_{r2} \frac{h}{d_a + 2h}. \quad (12)$$

With the help of fin efficiency, the current (external) heat transfer coefficient at the surface is

$$\alpha_0 = \frac{\alpha A_{tot}}{A_{tube} + \eta_r A_{fin}}. \quad (13)$$

The dimensionless number Nu_0 with a characteristic dimension $l' = d_a$ at the medium gas temperature is calculated using the established equation

$$Nu_0 = \frac{\alpha_0 d_a}{\lambda_{gm}}. \quad (14)$$

By taking into account an average mean boundary-layer temperature

$$T_b = \frac{T_{wall} + T_{gm}}{2}, \quad (15)$$

the Nusselt number is defined as:

$$Nu_b = Nu_0 \frac{\lambda}{\lambda_b}. \quad (16)$$

4.2 Governing pressure drop equations

The total pressure drop of the channel with inserts (tube bundle) is calculated using the following equation

$$\Delta p = N_R \xi \frac{\rho_{gm} w_E^2}{2}, \quad (17)$$

where ρ_{gm} and is the arithmetic mean density and w_E the velocity in the net free area of a row.

$$w_E = \frac{\dot{m}_g}{F_{min} \rho_{gm}} \quad (18)$$

The pressure drop coefficients of the channel were correlated using the Konakov [17] equation

$$\xi_{ch} = \frac{1}{(1.8 \log Re - 1.5)^2}. \quad (19)$$

The properties for the physical quantities are based on the arithmetic mean temperature of hot gas between inlet and outlet. By considering the pressure variation as a result of the temperature change over the bundle, the pressure drop coefficient for the serrated tube bundle is calculated as

$$\xi_{8R} = \left(\Delta p - \left(\frac{\dot{m}_g}{A_{ch}} \right)^2 \left(\frac{1}{\rho_{g1}} - \frac{1}{\rho_{g2}} \right) \right) \frac{2}{\rho_{gm} w_E^2} - 2\xi_{ch} \frac{L}{D_H}. \quad (20)$$

The average pressure drop coefficient for a single tube row is

$$\xi_{1R} = \frac{\xi_{8R}}{8}. \quad (21)$$

4.3 Measurement validation

The measurement uncertainties for the applied system are well known and have been specified. Each heat transfer measurement series is performed to attempt high accuracy. To obtain precise heat

transfer correlations, each calculated point was validated after measurement. The data validation model introduced by J. Tenner, P. Klaus and E. Schulze [21] was therefore applied. This curve-fitting technique utilizes equations for mass balances and energy balances as well as measurement value equations. The basic concept of the validation is to use all measurement values with their variances and co-variances to fulfil all side conditions. This criterion is developed as follows [21]:

The energy balance (1) and (2) is known and its conditions must be met. If we choose 6 measurement values for the variables m_w , m_g , T_{w1} , T_{w2} , T_{g1} , and T_{g2} , in these equations we obtain

$$\dot{Q} = M_1 c_{pw} (M_2 - M_3) \tag{22}$$

and

$$\dot{Q} = M_4 c_{pg} (M_5 - M_6) . \tag{23}$$

The real measurement values with their uncertainties

$$M = (M_1, M_2, M_3, \dots) \tag{24}$$

do not satisfy the side conditions. For this reason all of the measurement values are supplemented with correction factors. Thus we obtain the following:

$$V = M + v . \tag{25}$$

The correction factors v are determined in such a way that equation (26) reaches a minimum and the side condition (27) is equal to zero.

$$G(v) = v^T \sum M^{-1} v \rightarrow \text{Min} \tag{26}$$

$$h(V) = 0 \tag{27}$$

Equation (26) is the fitting function, with the inverse matrix for the co-variance. After combining equation (26) and (27) and using the Lagrange multiplier

$$\lambda = (\lambda_1, \lambda_2, \dots, \lambda_6), \tag{28}$$

we obtain

$$G(V, \lambda) = (V - M)^T \sum M^{-1} (V - M) + 2\lambda^T h(V) \rightarrow \text{Min} . \tag{29}$$

All measurement values are independent and the matrix of the co-variances according to [21], [22] is

$$\sum_{i=1}^6 M_i = \begin{vmatrix} \sigma_{M_1}^2 & & & & & \\ & \sigma_{M_2}^2 & & & & \\ & & \dots & & & \\ & & & & & \\ & & & & & \sigma_{M_6}^2 \end{vmatrix} . \tag{30}$$

After using the inverse co-variance matrix

$$\sum_{i=1}^6 M_i^{-1} = \begin{vmatrix} 1/\sigma_{M_1}^2 & & & & & \\ & 1/\sigma_{M_2}^2 & & & & \\ & & \dots & & & \\ & & & & & \\ & & & & & 1/\sigma_{M_6}^2 \end{vmatrix} , \tag{31}$$

for equation (29), it follows that

$$G(V, \lambda) = \frac{(V_1 - M_1)^2}{\sigma_{M_1}^2} + \dots + \frac{(V_6 - M_6)^2}{\sigma_{M_6}^2} + 2\lambda (V_1 c_{pw} (V_2 - V_3) - V_4 c_{pg} (V_5 - V_6)) \rightarrow \text{Min} . \tag{32}$$

The solution of equation (32) is known as calculus of variations with side conditions according to Gauss. A system of equations for 7 variables is obtained. The solutions to this system are the 6 validated measurement values and the Lagrange multiplier. For more details see [21] and [22]. After applying this condition, all measurement values can be developed into correlations for the prediction of the Nusselt number.

5 Comparison with other studies

5.1 Heat transfer correlations

Following dimensional analysis, the power law for the heat transfer correlation was developed.

$$Nu = K Re^m Pr^n \tag{33}$$

The objective function of Nusselt is defined as

$$Nu = f(Re, Pr) . \tag{34}$$

As known from the power law, the correlation of Escoa for external heat transfer at finned tubes with serrated fins in staggered arrangement of tubes is defined as

$$Nu = \frac{1}{4} Re^{0.65} Pr^{1/3} \left(\frac{T_{gm}}{T_s} \right)^{1/4} \left(\frac{d_a + 2h}{d_a} \right)^{1/2} C_3 C_5. \quad (35)$$

For the definition of C_3 , C_{3sol} , and C_5 see the literature in [2] and [15]. In case of solid finned tubes, C_{3sol} is applied in the place of C_3 for the calculation.

For the determination of external heat transfer, some correlations in the literature exist for solid or serrated finned tubes. Equations only for finned tubes with serrated and solid fins were developed by e.g. Escoa (Extended Surface Corporation of America) as well as by Nir [5]. The limitations of each of these functions (C_3 , C_{3sol} , and, C_5) can be found in [2] and [15]. Figure 6 shows the dimensionless heat transfer coefficient for a representative number of measured points in the Re-range of eight serrated and solid finned-tube rows in staggered arrangement. The heat transfer coefficient of the serrated I-shaped finned tube is somewhat greater than that for the U-shaped finned tube.

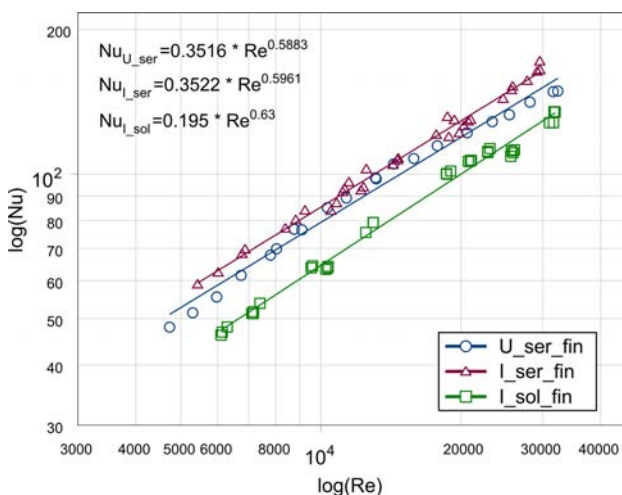


Fig.6: Heat transfer at 8 tube rows, Pr=0.71, serrated and solid tubes, d=38 mm

The curves for the serrated U-shaped and the I-shaped finned tubes show approximately the same gradient. The exponents for the Nusselt correlations vary from 0.53 to 0.65.

This variation could be caused by the pressure difference measurement uncertainty of the mass flow of air at low Re numbers and the temperature measurement uncertainty. Overall heat transfer of the solid finned tubes is inherently less. This is due to the effect of lower turbulences between the tubes. All I-shaped finned tubes have almost the same fin height and the same transversal and longitudinal pitch. Thus, there is no effect of a greater overall

heat transfer caused by the larger surface. Figure 7 presents the comparison of the measured results with literature.

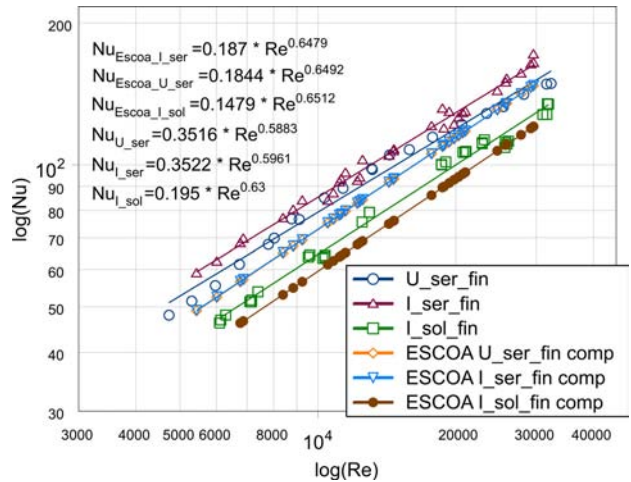


Fig.7: Comparison of heat transfer at 8 tube rows with literature, Pr=0.71, d=38 mm

As the comparison shows, fin segmentation intrinsically increases heat transfer. The measured results for the solid finned tubes show better agreement with the correlation in literature.

The equations of Weierman [2] and [15] have a measurement uncertainty of about $\pm 10\%$ for staggered layout. Thus, our results concur well with the literature.

Since in (35)

$$Nu = f(Re, Pr, \vartheta_{gm}, \vartheta_s, d_a, h, t_s, t_q, t_l) \quad (36)$$

and heat conduction through the tube and the fin varies for the two geometries, the formula for the Nusselt number has to be modified to reflect the same conditions. This objective function depends on parameters such as dimensionless groups, temperatures and geometry.

C_5 does not change in value due to equal transversal and longitudinal pitch. Each point in the diagram is obtained at different temperatures. For further calculations, a new average reference temperature for gas and fin has to be set. The Nusselt number then becomes

$$Nu_c = Nu_U \left(\frac{T_{gf}}{T_{sf}} \right)_I^{1/4} \sqrt{\frac{d_a + 2h_I}{d_a + 2h_U}} \frac{C_{3I}}{C_{3U}}. \quad (37)$$

C_3 and C_{3sol} are functions with the negative factor $h/(t-s)$ in the exponent. The influence of the factor $h/(t-s)$ on heat transfer is of interest. Its exact definition is given in [2] and [15].

A comparison among serrated fins reveals the following: if equation (37) is applied to the left side of (35), the factor $h/(t-s)$ calculates to 8.75 for U-shaped fins and to 5.31 for I-shaped fins. C_3 directly influences heat transfer. If the exponent $h/(t-s)$ is decreased, C_3 increases and overall heat transfer rises to 6.5%.

Figure 8 shows the relative deviation of our measured values for Nu from the Escoa correlations for the tested geometries (marked with Δ and \square). The points marked with \diamond in Figure 8 represent values for the relative deviation of the compared Nusselt numbers for U- and I-fin geometry with average reference temperatures. All points marked with \circ in Figure 8 represent values for the relative deviation of the compared Nusselt numbers for U-shaped and I-shaped fin geometry with exact measurement temperatures. All Nu correlations are calculated at constant Pr values. The Pr value represents the thermo-physical properties. In the case of air as heat transfer medium, the thermal boundary layer is thicker than the boundary layer with fluid flow. The variation of Pr under test conditions is small and can therefore be neglected in further calculation.

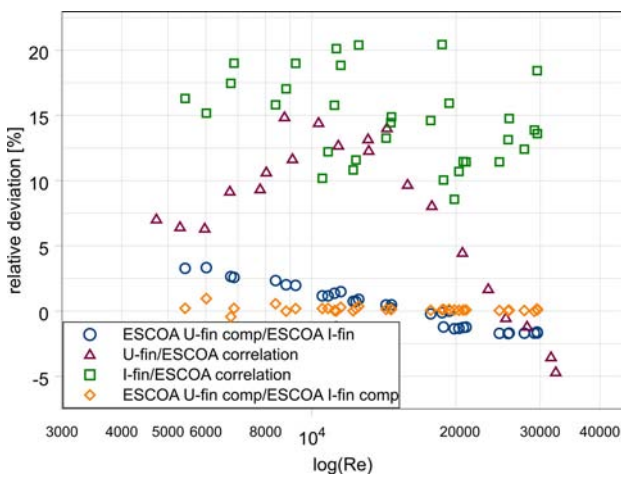


Fig.8: Relative deviation of correlations

As expected, the heat transfer coefficient declines with increasing fin height and fin pitch. Specifically, in view of Weiermans correlations, fin height does not very strongly influence overall heat transfer [8]. Yet with increasing fin height, the total external heating surface also increases. There could be a gain from the heating surface as h is increased. The volumetric heat capacity of a heat exchanger

with a U-shaped finned-tube bundle of the same longitudinal and transversal pitch, same number of tubes, smaller fin pitch and greater fin height is better than that of an I-shaped finned-tube bundle of the same installation size but with greater fin pitch (number of fins per meter).

The literature study shows an enhanced effect on heat transfer with variation of the fin height (see [8]). Most of the formulas included there have been developed for solid finned tubes. A comparison shows similar characteristics, as seen in [8]. The maximum fin height and the minimum fin pitch result from limitations, such as the need to avoid fouling, posed in finned-tube production by the kind of fuel used (liquid, solid or gaseous). In D.R. Reid and J. Taborek [1], recommended fin densities in relation to fuel type are presented.

5.1 Comparison of solid and serrated I-shaped finned tubes

Using the exponent $h/(t-s)$, a comparison between almost equal serrated and solid I-shaped finned tubes show an increase of C_3 . Therefore, C_{3sol} in the equation for solid finned tubes (15) is considered.

Overall heat transfer rises by about 22%. In Figure 9, this comparison of Nu at serrated and solid I-shaped finned tubes is presented for 13 validated measurement points. For a given fin height at $h/(t-s) = 5.718$ a scatter plot, marked with \square , is shown. This variation occurs due to measurement uncertainty when calculating the heat transfer rate. The calculated mean value \diamond for a comparison of the two different fin types shows good predictive capability for the increase in heat transfer rate according to equation (35).

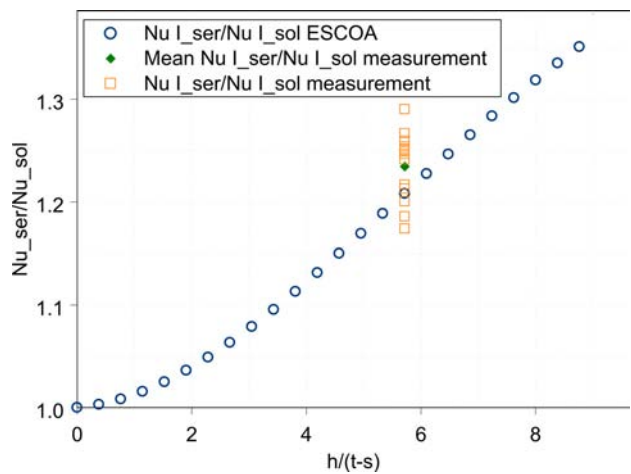


Fig.9: Comparison of serrated and solid I- fins.

As the comparison of the serrated and solid finned tubes in Figure 9 shows, the dimensionless heat transfer coefficient for 8 serrated finned tube rows in staggered arrangement is greater than that for the solid tube bundle. Fin segmentation increases turbulences, while gas penetration to the fin root area is improved (cf. Reid and Taborek [1]).

During manufacturing, the solid fin is stretched on the outside and compressed or shaped in a wave-like manner on the inside. The choice of the strip steel for the fins is thus restricted to very ductile materials. Serrated finned tubes are easier to manufacture using the high-frequency resistance welding technique.

5.2 Comparison of solid I-shaped finned tubes with literature

For the evaluation of the external heat transfer coefficient of finned tubes, measurements were performed using the method of T. E. Schmidt [23]. According to T. E. Schmidt, in terms of significance, taking into account the bare tube diameter as a variable for determining heat transfer at finned tubes is compensated by the addition of the area ratio. The constants are average values resulting from a large number of test cases, mostly with annular fins, which result in lower heat transfer coefficients than spiral fins (see Figure 10). In the latter case, the constants might be increased by approximately 10% [8]. Pursuing another course, Brandt [32] uses the flooding length as the characteristic length. In addition, an arrangement factor has to be calculated, in this case using the remaining geometrical data. FDBR (Fachverband Dampfkessel-, Behaelter- und Rohrleitungsbau) [33] selects for the characteristic length the equivalent “in-area” diameter according to Schmidt.

A further equation for heat transfer at staggered finned-tube bundles is specified in the VDI Waermeatlas, 7th edition [34]. This equation uses the bare diameter as the characteristic length. Vampola’s equation, cited in [8], is valid for staggered finned-tube bundles. He uses a characteristic length which is derived from the tube diameter and an equivalent fin diameter, with a weighted average value for the bare tube surface and the fin surface. All of these correlations along with scope of validity are described in [8].

As Figure (10) shows, the results of the measurement at solid I-shaped finned tubes lie within the range of the other equations, developed for solid spiral finned tubes, in the literature.

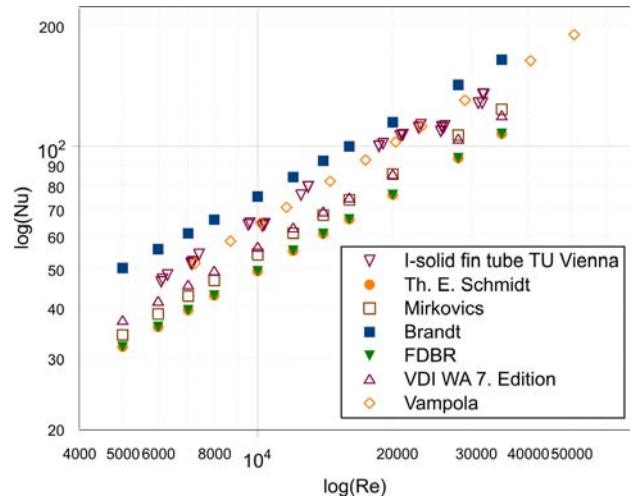


Fig.10: Comparison with literature: heat transfer at 8 tube rows, Pr=0.71, solid I-shaped tubes, d=38mm

5.3 Pressure drop coefficient correlations

The pressure drop coefficient correlation is defined according to Escoa as

$$\xi = 4 \left(\frac{d_a + 2h}{d_a} \right)^{1/2} C_2 C_4 C_6 \quad (38)$$

For the definition of C_2 , C_4 , and C_6 , see the literature in [2] and [15]. A comparison of the two heat exchanger geometries is only possible at the same conditions. The objective function for pressure drop is

$$\xi = f(\text{Re}, N_R, d_a, h, t, s, t_1, t_q) \quad (39).$$

This accounts for dimensionless groups, tube row numbers and the geometry. For ξ_c , the equation

$$\xi_c = \xi_U \left(\frac{d_a + 2h_U}{d_a + 2h_U} \right)^{1/2} \frac{C_{4I}}{C_{4U}} \quad (40)$$

is obtained. In Figure 11, the pressure drop coefficient for 8 tube rows in staggered arrangement is shown. The index ξ indicates the position of the measurement. ξ_1 (zeta1) is calculated from the static pressure differences on the air side at the finned-tube bundle wall, where ξ_2 (zeta2) is calculated from total pressure differences in the centre of the channel. No flow separation or bypass flow could be detected.

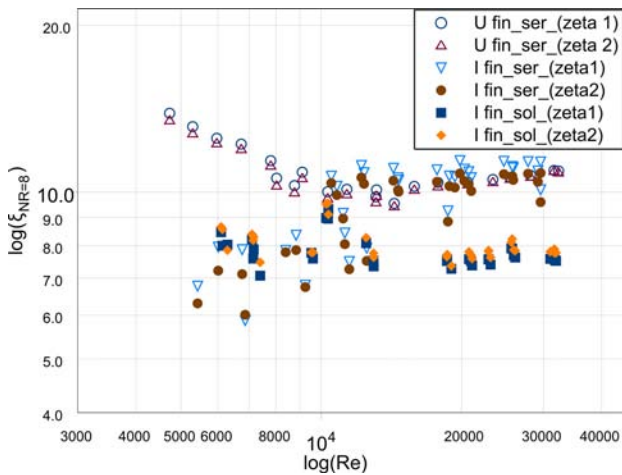


Fig.11: Pressure drop coefficient for 8 tube rows

For $Re > 10000$ the pressure drop coefficient of the three finned-tube bundles has the same characteristics, while for $Re < 10000$ great uncertainty is revealed for the small pressure difference among I-shaped finned tubes. For $Re \geq 15000$, a small increase takes place, then, at $25000 < Re < 35000$, the pressure drop coefficient tends to show a constant value. The pressure drop at the solid test tubes is higher for the measured Re -range than is calculated with equation (38) (see Figure 12). The U-shaped finned tubes have the same gradient as the Escosa correlation for $Re < 15000$. ξ has approximately the same values for $8000 < Re < 10000$. The influence of fin height on the pressure drop at the same installation size indicates an increase of the pressure drop coefficient with h according to all relations in [8]. This is due to less net free area in a tube row, which influences w_E in equation (18) and the pressure drop in (17).

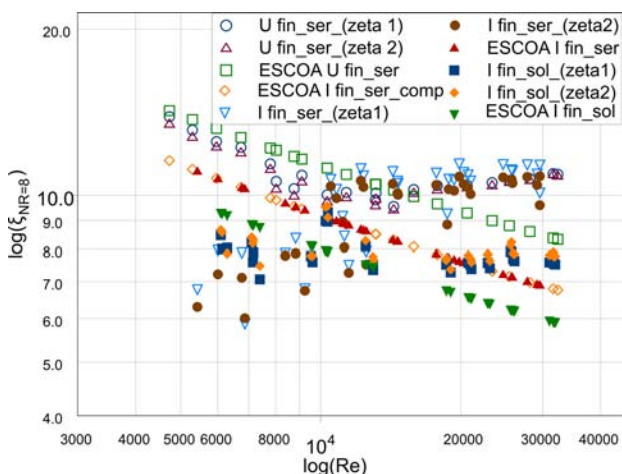


Fig.12: Comparison of pressure drop coefficient for 8 tube rows with literature

Although the fin height varies among the various serrated geometries tested, the net free area in a tube row is nearly the same in each case. Thus, a significant difference among pressure drop coefficients is not expected. As the overall heat transfer at solid fin tubes is around 20% lower than for serrated fin tubes, the pressure drop shows the same tendencies.

6 L ev eque Analogy for finned tubes

An analogy exists between pressure drop and heat transfer for tube bundles based on the “generalized L ev eque equation” [13]. To calculate heat transfer in cases of known pressure drop, the equation is defined as follows

$$\frac{Nu}{Pr^{1/3}} = 0.404 \cdot \left(x_f \xi_{IR} Re_h^2 \frac{d_h}{L} \right)^{1/3}, \tag{41}$$

where x_f ($= 0.46$) is a factor according to [13], ξ_{IR} the pressure drop coefficient for a single tube row, d_h the hydraulic diameter ($d_h = 4A/U$) and L the diagonal pitch of the longitudinal and transversal pitch for staggered arrangements. For more details, refer to [13]. The use of this criterion aids in evaluating the uncertainty of the pressure drop measurement through a comparison of the heat transfer calculation and the L ev eque equation. Figure 13 shows the characteristics for I-shaped and U-shaped finned-tube bundles based on ξ_1 and ξ_2 . A comparison with the calculated heat transfer correlation in Figure 7 reveals good correlation.

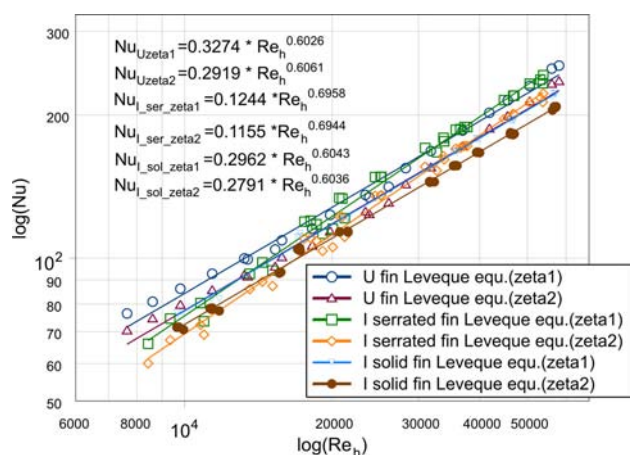


Fig.13: L ev eque equations according to [13]

The exponents of U-shaped finned tubes are almost the same, while differences could be identified between the exponents of the calculated heat transfer correlations and the L ev eque equations

for I-shaped finned tubes with regard to the uncertainty of the pressure difference measurement for $Re < 10000$. In this case heat transfer for $Re < 10000$ is underestimated.

All pressure drop measurements were carried out at augmented temperatures. Good agreement for the prediction of heat transfer correlations according to the L ev eque equation can be seen. This criterion seems to be valid for finned-tube bundles as well and generally indicates low uncertainty in pressure drop measurements with our arrangement.

7 Performance comparison of I-shaped and U-shaped finned tubes

The three different heat exchangers are compared in order to identify the best performance. Specifically, the pressure drop characteristic and the heat transfer characteristic are indirectly proportional. The objective is to identify a Reynolds number for the "best point". Several criteria for the evaluation of the performance of a heat exchanger can be found in literature (see [8], [16]).

By way of example, the criteria suggested and developed by Webb for single-phase flow [14] was used.

$$\frac{(\alpha^* A^*)/(\alpha A)}{(P^*/P)^{1/3} / (A^*/A)^{2/3}} = \frac{j^*/j}{(\xi^*/\xi)^{1/3}} = \frac{(St^* Pr^{*2/3})/(St Pr^{2/3})}{(\xi^*/\xi)^{1/3}} \tag{42}$$

The terms on the left of this equation, $(\alpha^* A^*)/(\alpha A)$, $(P^*/P)^{1/3}$ and $(A^*/A)^{1/3}$, are part of the Colburn factor ratio for heat transfer and the pressure drop ratio, whereby

$$St = \frac{Nu}{Re Pr} = \frac{\alpha}{\rho_{gm} c_{p_{gm}} w_{gm}} \tag{43}$$

Enhanced heat transfer is only achieved using finned tubes by means of an increase in pressure drop. Three different possibilities are described by this criterion:

- I. $(\alpha^* A^*)/(\alpha A)$...maximizing the heat transfer rate for equal P^*/P and A^*/A ;
- II. P^*/P ...minimizing the pumping power for equal $(\alpha^* A^*)/(\alpha A)$ and A^*/A ;
- III. A^*/A ...minimizing the overall heat exchanger size for equal P^*/P and $(\alpha^* A^*)/(\alpha A)$.

Ad (I): Maximizing the heat transfer rate

It is assumed that the investigated heat exchanger has equal pumping power and equal overall heat exchanger size. For equation (42) it follows that:

$$(\alpha^* A^*)/(\alpha A) = \frac{(St^* Pr^{*2/3})/(St Pr^{2/3})}{(\xi^*/\xi)^{1/3}} \tag{44}$$

At equal installation size, an increase of the heat transfer surface area, and thus of the heat transfer rate, is only achieved at the expense of an increase in pressure drop. Optimizing the heat exchanger by means of the performance criterion entails maximizing the heat transfer rate while simultaneously minimizing pressure drop and heat exchanger size. As the comparison between solid and serrated finned tubes in Figure 14 shows, the heat transfer rate for serrated I-shaped fins increases significantly for $Re < 10000$. For $Re > 15000$ the heat transfer rate, at 1.2, tends to display a constant value. This equals the value calculated using equation (35).

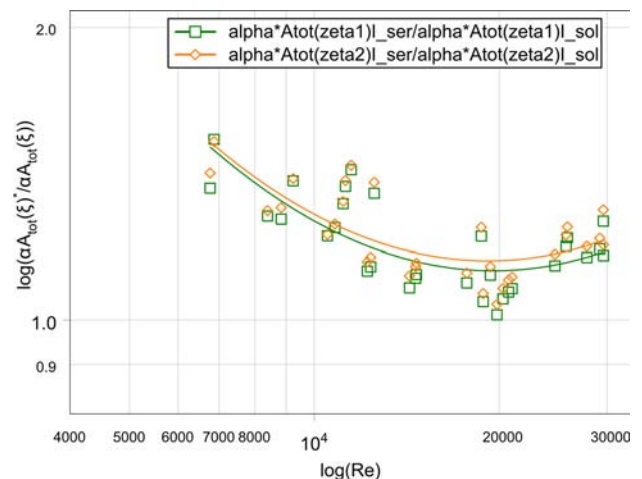


Fig.14: $(\alpha^* A^*)/(\alpha A)$ for serrated/solid I-shaped fins, equal P^*/P and A^*/A

A comparison of the different serrated finned tubes is presented in Figure 15. The heat transfer rate for serrated I-shaped and U-shaped fins increases for $Re < 10000$ and $Re > 20000$. This effect is more pronounced for low Re numbers. Between $10000 < Re < 20000$, no significant difference can be identified.

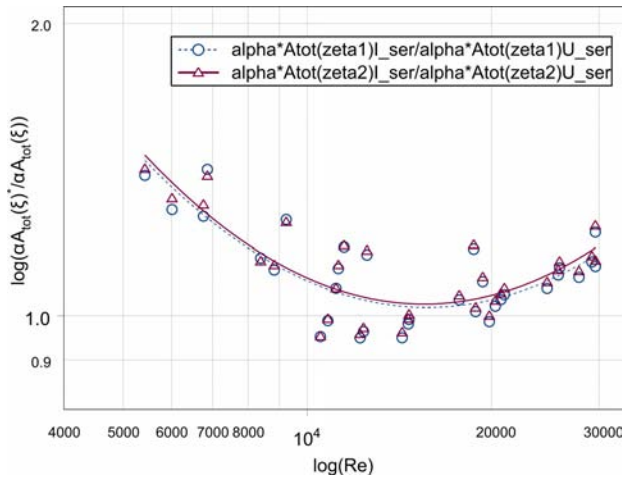


Fig.15: $(\alpha^* A^*)/(\alpha A)$ for equal P^*/P and A^*/A

Ad (II): Minimizing the pumping power

For equal heat transfer rate and equal overall heat exchanger size, equation (42) can be written as follows:

$$\frac{1}{(P^*/P)^{1/3}} = \frac{(St^* Pr^{*2/3})/(St Pr^{2/3})}{(\xi^*/\xi)^{1/3}} \quad (45)$$

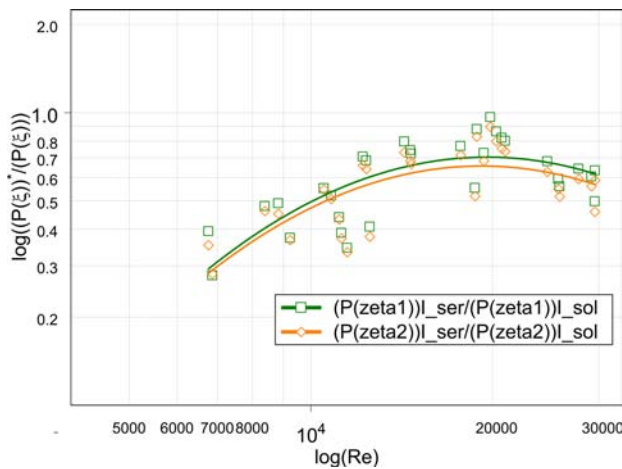


Fig.16: P^*/P for serrated/solid I-shaped fins, equal $(\alpha^* A^*)/(\alpha A)$ and A^*/A

The pumping power (Figure 16) of the serrated I-shaped finned tubes is lower for $Re < 10000$ and $Re > 20000$. At $Re = 20000$ the pumping power is almost the same as with solid finned tubes. All solid finned tubes show higher P . This kind of tube has a relatively low h and almost equal A_{sol} compared to A_{ser} . Satisfying condition (II) at equal $(\alpha^* A^*)/(\alpha A)$ and A^*/A results in an increase in pumping power. This effect might be intensified by the high measurement uncertainty at low Re numbers, as mentioned above.

A comparison of all serrated finned tubes under condition (II) is seen in Figure 17. With $Re < 10000$ and $Re > 20000$, pumping power increases for all tubes. In the range of $10000 < Re < 20000$, pumping power displays the same characteristic curve for both serrated U-shaped and I-shaped finned tubes. The small difference resulting from the varying net free area in tube rows with these tube geometries was neglected. This difference is about 3.36%.

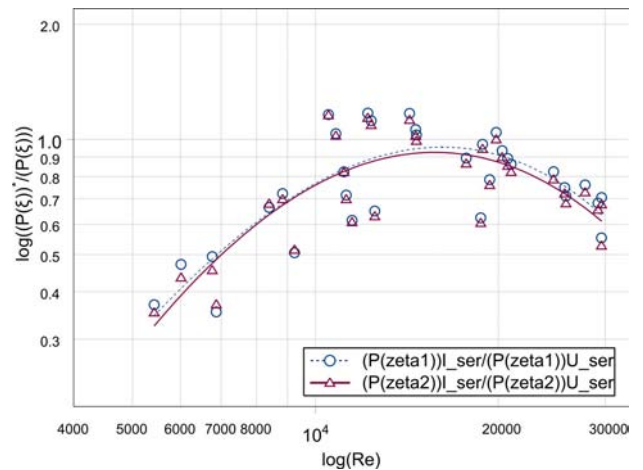


Fig.17: P^*/P for equal $(\alpha^* A^*)/(\alpha A)$ and A^*/A

Ad (III): Minimizing the overall heat exchanger size

The ratios of the heat transfer rate and pumping power are assumed to be 1. Thus, the following holds:

$$\frac{1}{(A^*/A)^{2/3}} = \frac{(St^* Pr^{*2/3})/(St Pr^{2/3})}{(\xi^*/\xi)^{1/3}} \quad (46)$$

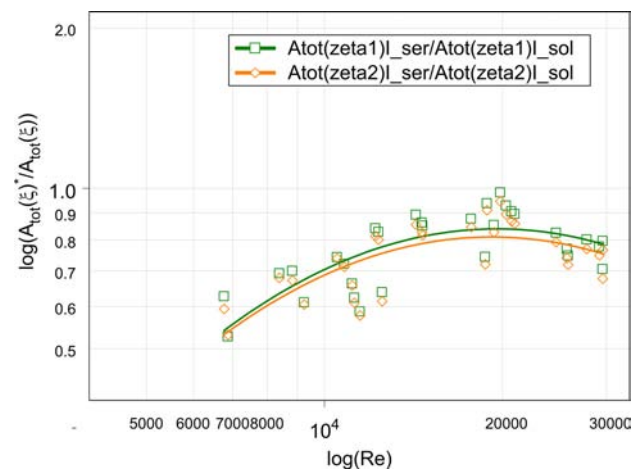


Fig.18: A^*/A for serrated/solid I-shaped fins, equal P^*/P and $(\alpha^* A^*)/(\alpha A)$

The two I-shaped finned-tube bundles are considered first: In Figure 18, the ratio of the total outside surface area of the bundles is presented. The α values for the two heat exchangers vary only little. To enhance heat transfer, it is necessary to enlarge the tube surface area and/or improve heat conduction.

Within the Reynolds range investigated, an enhanced system is achieved using a solid finned tube.

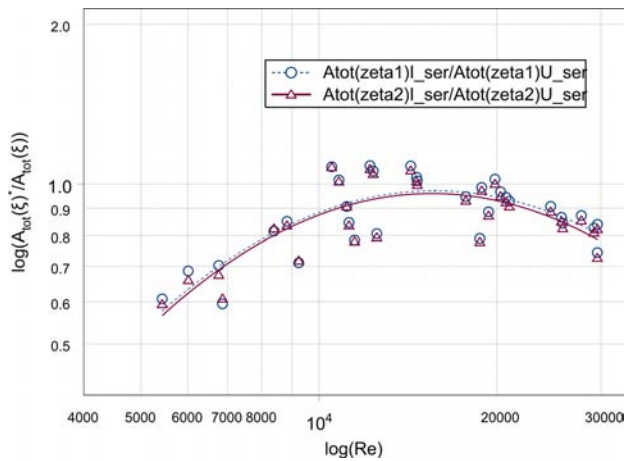


Fig.19: A^*/A for equal P^*/P and $(\alpha^* A^*)/(\alpha A)$

Yet for $Re < 10000$ and $Re > 20000$ the installation size of the heat exchanger with U-shaped fins is superior (refer to Figure 19). In the range of $10000 < Re < 20000$ no improvement of the heat exchanger size is possible. This inverse result is due to the constant transverse and longitudinal pitch. As the finned tubes have almost the same net free area within one tube row, only the packing density of the heat exchangers differs.

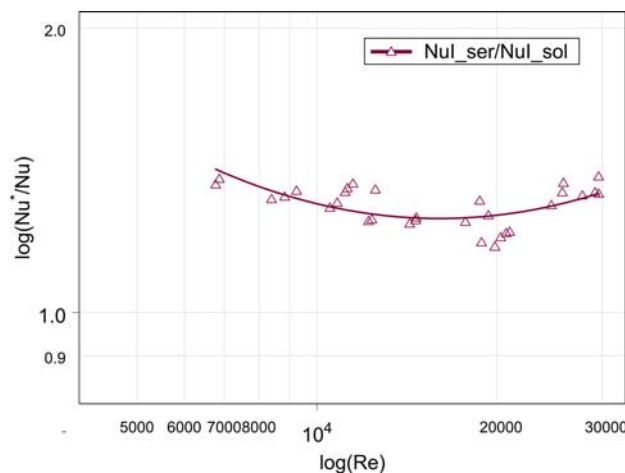


Fig.20: Ratio solid/serrated Nu_I of investigated tubes

All serrated I-shaped finned tubes would require less space than U-shaped finned tubes. Yet this result is obtained only for the same tube pitch.

In Figure 20, the ratio of Nusselt numbers for the tubes with I-shaped fins is shown. The segmentation of the fin may be seen to increase the dimensionless heat transfer coefficient within the investigated Reynolds range.

For $Re < 10000$ and $Re > 20000$, this effect is even more significant. Moreover, a comparison of serrated I-shaped and U-shaped finned tubes reveals superior results using I-shaped fins with a fin height of 15 mm (Fig. 21).

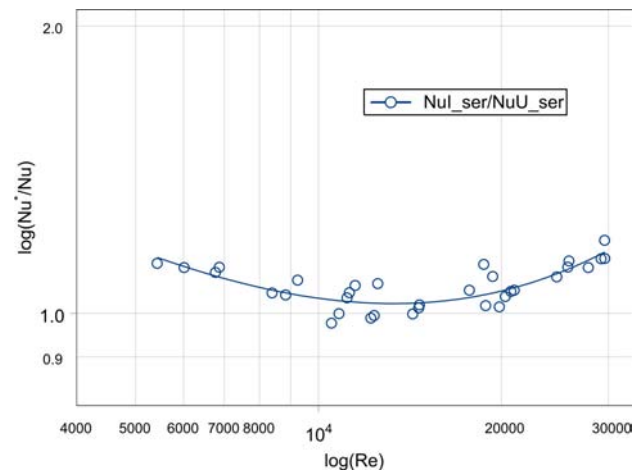


Fig. 21: Ratio Nu_I/Nu_U for serrated tubes

This relation does not take into account variations in heat conduction between U-shaped and I-shaped fins. In the range of $10000 < Re < 20000$, serrated heat exchangers display very similar behaviour; no advantage in terms of pumping power or heat exchanger surface area could be observed for this range. This leads us to conclude that fin height is apparently the single most important factor for evaluating the performance of the investigated finned tube geometries.

8 Conclusion

Experimental studies were performed to compare heat transfer and pressure drop correlations of serrated and solid finned tubes as well as the influences of various geometric parameters such as fin height. Following an analysis and evaluation of the measured values, heat transfer and pressure drop correlations were determined. A comparison with correlations from the literature revealed good congruence with little uncertainty. A comparison of the investigated fin tubes with the literature also revealed a decrease in heat transfer with greater fin

height. Thus, an optimum fin height can be determined and/or achieved, e.g. by using second law analysis. A comparison with the L ev e equation revealed good predictive ability for the Nusselt number at given pressure drop values. A performance evaluation criterion for single-phase flows was applied to characterize the efficiency of the various finned-tube bundles. Upon comparing serrated finned tubes, three ranges could be identified: $Re < 10000$, $10000 < Re < 20000$ and $Re > 20000$. Despite varying fin height and fin pitch in the two different geometries, no substantially differing tendencies could be observed when applying these equations.

A comparison of solid and segmented finned tubes revealed a general increase in the air-side heat transfer coefficient within the investigated Reynolds range. The validated measurement values for solid and serrated I-shaped finned tubes displayed good agreement with the formulas in the literature.

All of these results represent the first step in evaluating heat exchanger performance using our experimental technique.

As a next step, further studies of geometrical constants in the objective functions (36) and (39) will be carried out in order to identify any additional influences on heat transfer and pressure drop, i.e. fin height, fin pitch, fin thickness and fin width. In addition, the influence of the differences between solid and serrated finned tubes should be analyzed, specifically the effects resulting from differing fin heights, using various correlations from literature. Second law analysis could be applied, for example, as a criterion for optimizing performance (geometric parameters). Only little data is provided in literature regarding the influence on the heat transfer coefficient of varying the number of tubes arranged consecutively (see [27]). A further step would be to investigate various finned-tube arrangements with only few tube rows.

Moreover, the numerical investigation of local heat transfer behaviour in a single tube row when turbulences (e.g. horseshoe vortices) occur in the fluid flow between the fin tips represents a very promising subject of study. Measurement results of global performance could be compared with these calculations. Furthermore, knowledge of fluid flow and local heat transfer distribution will provide a more complete understanding of performance behaviour.

9 Nomenclature

A	Surface area	$[m^2]$
A_{fin}	Fin surface area of the bundle	$[m^2]$

A_{tube}	Bare tube surface area of the finned-tube bundle	$[m^2]$
A_{tot}	Total outside surface area of the finned-tube bundle	$[m^2]$
b_s	Segment width	$[m]$
c_p	Specific heat capacity	$[J/kgK]$
d_a	Bare tube diameter	$[m]$
D_H	Hydraulic diameter	$[m]$
f_a	Geometry factor	$[-]$
F_{min}	Minimum net free area in a tube row	$[m^2]$
$G(\nu)$	Fitting function	-
$h(\nu)$	Side function	-
h	Average fin height	$[m]$
h	Specific enthalpy	$[J/kg]$
h_{red}	Reduced fin height for the radian part with the segment	$[m]$
h_{red2}	Reduced fin height for the radian part without the segment	$[m]$
k	Heat transfer coefficient	$[W/m^2K]$
L	Diagonal pitch	$[m]$
\dot{m}	Mass flow	$[kg/s]$
m_1	Parameter for the fin efficiency	$[1/m]$
m_2	Parameter for the fin efficiency	$[1/m]$
$M_{1..6}$	Measurement values	
N_R	Number of tubes in the flow direction	$[-]$
p	Pressure	$[N/m^2]$
Δp	Pressure drop	$[N/m^2]$
\dot{Q}	Heat transfer rate	$[W]$
s	Average fin thickness	$[m]$
t	Fin pitch	$[m]$
t_l	Longitudinal tube pitch	$[m]$
t_q	Transverse tube pitch	$[m]$
T	Temperature	$[K]$
ΔT_{ln}	Logarithmic mean temperature difference (LMTD)	$[K]$
T_s	Average fin temperature	$[K]$
U	Circumference	$[m]$
V	Corrected measurement value	
\dot{V}	Volume flow	$[m^3/h]$
w_E	Velocity in the net free area of a tube row	$[m/s]$
w_w	Velocity of water	$[m/s]$
x_F	Factor according to [13]	$[-]$
j	Colburn factor	$[-]$
Nu	Nusselt number	$[-]$
Pr	Prandtl number	$[-]$
Re	Reynolds number	$[-]$
St	Stanton number	$[-]$

Greek Symbols

α	Heat transfer coefficient	$[W/m^2K]$
η_r	Fin efficiency	$[-]$

η_{r1}	Fin efficiency for the radian part with the segment	[-]
η_{r2}	Fin efficiency for the radian part without the segment	[-]
λ_r	Thermal conductivity of fin	[W/mK]
λ	Thermal conductivity	[W/mK]
$\lambda_{1..6}$	Lagrange multiplier	-
υ	Correction	-
ρ	Density	[kg/m ³]
$\sigma_{M1..6}$	Co-variances	[-]
ξ	Pressure drop coefficient	[-]

Indices

0	Characteristic length at d_a
1	Inlet
2	Outlet
8R	8 tube rows
1R	Single tube row
a	Outside
b	Calculation condition
c	Converted
ch	Channel
f	Fix
g	Gas
h	Hydraulic
i	Inside
I, U	Shape of finned-tube
m	Average mean
K, m, n	Function on geometric parameters and tube-bundle arrangement in equ. (33)
min	Minimum
s	Serrated I-shaped tube
sf	Fin fixed
sol	Solid
ser	Serrated
tot	Total
w	Water

References:

- [1] D.R. Reid, J. Taborek, Selection criteria for plain and segmented finned tubes for heat recovery systems, *Transactions of the ASME*, Vol.116, 1994, pp. 406-410.
- [2] C. Weierman, Correlations ease the selection of finned tubes, *The Oil and Gas Journal*, Vol.74, No.36, 1976, pp. 94-100.
- [3] C. Weierman, J. Taborek, W.J. Marner, Comparison of the performance of in-line and staggered banks of tubes with segmented fins, *The American Institute of Chem. Engineers*, Vol.74, No.174, 1978, pp. 39-46.
- [4] S.P. Kearney, A.M. Jacobi, Local convective behavior and fin efficiency in shallow banks of in-line

and staggered, annularly finned tubes, *Journal of Heat Transfer*, Vol.118, 1996, pp. 317-325.

- [5] A. Nir, Heat transfer and friction factor correlations for cross flow over staggered finned tube banks, *Heat Transfer Eng.*, Vol.12, No.1, 1991, pp. 43-58.
- [6] F. Frasz, Waermeuebertragung in Rippenrohr-waermeaustauschern, *Waermeaustauscher, Energieeinsparung durch Optimierung von Waermeprozessen*, Vulkan-Verlag Essen 2, 1994, pp. 70-76.
- [7] K. Kawaguchi, Heat transfer and pressure drop characteristics of finned tube banks in forced convection, *Journal of Enhanced Heat Transfer*, Vol.12, No.1, 2005, pp. 1-20.
- [8] F. Frasz, Principles of finned-tube heat exchanger design for enhanced heat transfer, *Heat and Mass Transfer*, WSEAS-Press, 2008.
- [9] H. Walczyk et al, An experimental study of convective heat transfer from extruded type helical finned tubes, *Chemical Engineering and Processing*, Vol.42, 2003, pp. 29-38.
- [10] F. Halici, I. Taymaz, Experimental study of the airside performance of tube row spacing in finned tube heat exchangers, *Heat and Mass Transfer*, Vol.42, 2006, pp. 817-822.
- [11] E. Næss, Heat transfer and pressure drop in serrated-fin tube bundles for waste heat recovery applications, *6th World Conference on Experimental Heat Transfer, Fluid Mechanics, and Thermodynamics*, 2005, Japan, No.1-a-14, pp.1-5.
- [12] K. Hashizume et al, Fin efficiency of serrated fins, *Heat Transfer Engineering*, Vol.23, 2002, pp. 6-14.
- [13] H. Martin, V. Gnielinski, Calculation of heat transfer from pressure drop in tube bundles, *3rd European Thermal Sc. Conf. 2000*, pp. 1155-1160.
- [14] R.L. Webb, *Principles of enhanced heat transfer*, John, Wiley&Sons, 1994.
- [15] ESCOA Turb-X HF Rating Instructions, ESCOA, Pryor, Oklahoma, 1979.
- [16] K. Stephan, J. Mitrović, Massnahmen zur Intensivierung des Waermeuebergangs, *Chemie Ingenieur Technik*, 56, Nr.6, 1984, pp. 427-431.
- [17] P.K. Konakov, Eine neue Formel fuer den Reibungskoeffizienten glatter Rohre, *Bericht der Akkademie der Wissenschaften der UDSSR*, Vol. 51, Nr.7, 1954, pp. 503-506.
- [18] S.B. Genic et al., Research on air pressure drop in helically-finned tube heat exchangers, *Applied Thermal Engineering*, Vol. 26, 2006, pp. 478-485.
- [19] T.J. Rabas, P.W. Eckels, Heat transfer and pressure drop performance of segmented extended surface tube bundles, *AICHE-ASME Heat Transfer Conference, San Francisco, California, Aug.11-13, 1975, pp. 1-8.*

- [20] R.L. Webb, Air-side heat transfer in finned tube heat exchangers, *Heat Transfer Engineering*, Vol. 1, Nr. 3, 1980, pp. 33-49.
- [21] J. Tenner, P. Klaus, E. Schulze, Erfahrungen bei der Erstellung und dem Einsatz eines Datenvalidierungsmodells zur Prozessueberwachung und -optimierung im Kernkraftwerk Isar 2, *VGB Kraftwerkstechnik*, Vol. 4, 1998, pp. 43-49.
- [22] S. Streit, Messunsicherheit und Vertraeglichkeitspruefungen: Beispiele und vergleich mit herkoemmlichen Verfahren, *VDI-Bericht 1210*, 1995.
- [23] Th. E. Schmidt, Der Waermeuebergang an Rippenrohre und die Berechnung von Rohrbuendel-Waermeaustauschern, *Kaeltetechnik*, Vol.15, No.4, 1963, pp. 98-102.
- [24] R. G. Carranza, J. Ospina, Fin efficiency of a Three Sided Pyramidal Fin of Equilateral Triangular and Variable Cross-Sectional Area: Analytical Solution, *WSEAS Transactions on Heat and Mass Transfer*, Issue 3, Vol.1, 2006, pp. 337-341.
- [25] H. Necula, E. Nineta, G. Darie, An experimental analyse of heat transfer for a tube bundle in a transversally flowing air, *WSEAS Transactions on Heat and Mass Transfer*, Issue 3, Vol.1, 2006, pp. 349-355.
- [26] R.G. Carranza, Spine Fin Efficiency A Three Sided Pyramidal Fin of Scalene Triangular Cross-Sectional Area: Analytical Solution, *5th WSEAS Int. Conf. on Heat and Mass transfer (HMT'08)*, Acapulco, Mexico, January 25-27, 2008.
- [27] F. Frasz, W. Linzer, Waermeuebergangsprobleme an querangestromten Rippenrohrbuendeln, *BWK*, Vol.44, No.7/8, 1992, pp. 333-336.
- [28] D.E. Briggs, E.H. Young, Convection heat transfer and pressure drop of air flowing across triangular pitch banks of finned tubes, *Chem. Eng. Prog. Symp. Ser.*, Vol.59, No.41, 1963, pp. 1-10.
- [29] D.J. Ward, E.H. Young, Heat transfer and pressure drop of air in forced convection across triangular pitch banks of finned tubes, *Chem. Eng. Prog. Symp. Ser.*, Vol.55, No.29, 1959, pp. 37-44.
- [30] K.J. Bell, W.H. Kelger, Analysis of bypass flow effects in tube banks and heat exchangers, *The American Institute of Chem. Engineers*, Vol.74, No.174, 1978, pp. 47-52.
- [31] G. Breber, Heat transfer and pressure drop of stud finned tubes, *The American Institute of Chem. Engineers*, Vol.87, No.283, 1991, pp. 383-390.
- [32] F. Brandt, Waermeuebertragung in Dampferzeugern und Waermeaustauschern, *FDBR Fachbuchreihe Bd.2*, Vulkan Verlag Essen 1985.
- [33] FDBR Handbuch Waerme – und Stroemungstechnik, Waermeuebertragung in Dampferzeugern und Waermeaustauschern, *Fachverband Dampf-*
kessel-, Behaelter- und Rohrleitungsbau, Essen 1980.
- [34] VDI-Waermeatlas, *7th Edition*, VDI Verlag Duesseldorf 1994.